Observations of restratification after a wind mixing event in a shallow highly stratified estuary

Jeff Coogan[1], Brian Dzwonkowski[1], Kyeong Park[2], and Bret Webb[3]

[1]University of South Alabama, Dauphin Island Sea Lab, Dauphin Island, Alabama
[2] Department of Marine Sciences, Texas A&M University at Galveston, Galveston, Texas
[3] Department of Civil Engineering, University of South Alabama, Mobile, Alabama, USA.

Abstract In stratified estuaries susceptible to wind mixing events, the changes in stratification have important implications for estuarine dynamics. Understanding the time scale associated with these mixing events and indirect wind impacts is dependent on estimating the restratification time scale. Bay-wide stratification observations, turbulence timeseries, and long-term data were examined to quantify the response mechanisms and restratification times in Mobile Bay. Observations showed moderate increases in stratification occurred over 2-3 days after the mixing event and were spatially variable. Turbulence data and model results further highlight the period of returning stratification had changes in the relative contribution of tidal straining and gravitational exchange for the residual circulation in the estuary. Estimates of dissipation for the two ADVs averaged $2.6{-}3.1 \times 10^{-5}\ m^2\ s^{-3}$ prior to the mixing event and increased to $1.4{-}8.5 \times 10^{-4}\ m^2\ s^{-3}$ after the mixing event. These changes showed with increasing stratification, the turbulent dissipation decreased. These results highlight initial high returns in stratification are slowed over time as the exchange and mixing in the bay develop and stratification returns to its premixed state.

Keywords Restratification, tidal straining, highly stratified, estuarine hydrodynamics, wind mixing

Corresponding author address: Department of Marine Sciences, University of South Alabama, Dauphin Island Sea Lab, 101 Bienville Blvd., Dauphin Island, AL 36528, USA.
E-mail: Jcoogan@disl.org

Introduction

Stratification in estuaries can be simply described as a balance between mixing components (e.g. wind and tidal energy) and stratifying components (e.g. advection of density gradients). From this balance, the changes in the vertical and horizontal salinity distribution for an estuary can be classified as: salt wedge, strongly stratified, partially mixed, and well mixed systems (Valle-Levinson 2010). These classifications highlight important physical differences between the systems due to the feedbacks between estuarine exchange and salt flux associated with changing stratification. Strongly stratified systems are characterized by a well-developed pycnocline and 2-layer circulation with relatively weak inflow. Partially mixed systems exhibit a weak pycnocline or continuous stratification with the most vigorous 2-layer circulation whereas well mixed systems have mean flows that are unidirectional with depth and are often driven by tidal forcing.

Understanding this dynamic balance is important for quantifying the role of stratification on circulation. The coupled momentum and salt balance equations provide the bases of how estuaries function (Hansen and Rattray 1966; Pritchard 1956), and the two-dimensional (x-z) equations may be written as:

$$\frac{1}{\rho}\frac{\partial p}{\partial x} = A_z \frac{\partial^2 u}{\partial z^2} \tag{1}$$

$$\frac{\partial s}{\partial t} + u\frac{\partial s}{\partial x} = \frac{\partial}{\partial z}\left(K_z \frac{\partial s}{\partial z}\right) \tag{2}$$

where t is time, x and z are longitudinal and vertical coordinates, respectively, ρ is the density, $\partial p/\partial x$ is the longitudinal pressure gradient, u is the longitudinal velocity, s is salinity, and A_z and K_z are the vertical eddy viscosity and diffusivity, respectively. The velocity from the momentum balance (Eq. 1) is dependent on changes in stratification through the eddy viscosity term. The velocity field then controls the advective salt flux in the salt balance (Eq. 2), leading to the coupled response, where changes in salt transport can impact stratification that feedbacks into the momentum balance. This coupled response has led to simple modeling challenges that result from runaway stratification. In strongly stratified systems, the parameterization of eddy viscosity can lead to runaway stratification, where straining of the salinity gradient exceeds mixing and leads to a continuous increase in stratification beyond realistic results (Geyer and MacCready 2014).

Understanding how stratification controls exchange dynamics can also improve our understanding of its role in biogeochemical processes and the transport of materials. Dissolved oxygen concentrations in estuaries have received significant scrutiny for the impact stratification has on limiting vertical exchange. Observations from Mobile Bay have

shown when salinity differences are less than 2 PSU (over 2.5 m) hypoxia rarely occurred, but when stratification exceeded 8 PSU hypoxia occurred almost all the time (Park et al. 2007). Stratification can also impact sediment transport through enhancing the trapping of suspended sediment and fate of these materials in estuaries (Geyer 1993).

The balance of mixing (R.H.S. of Eq. 2) and stratifying (straining of the salinity gradient) components can be parameterized by the Simpson number (*Si*) or horizontal Richardson number (Stacey et al 2001):

$$Si = \frac{N_x^2 H^2}{U_{*b}^2} \tag{3}$$

where $N_x^2 = -g\beta\partial s/\partial x$ is the horizontal buoyancy frequency, g is gravity, β is the saline contraction coefficient, U_{*b} is the bottom friction velocity and H is depth. As *Si* increases the mixing component is overtaken by the strain induced stratification and leads to stratified conditions. Changes in *Si* and stratification have been observed over spring-neap cycles and can lead to periods of well mixed and stratified changes in estuaries (MacCready and Geyer 2010). Restratification timescales between these mixed and stratified periods have been observed in the Hudson River as occurring rapidly (Geyer et al. 2000), but Geyer and MacCready (2014) reported other works that showed longer lags in restratification times. In addition to tidal mixing, wind can also play an important role in this mixing/stratifying balance. Chen and Sanford (2009) modified *Si* to include wind mixing and straining components. From this new balance, stratification in estuaries can change not only during spring-neap cycles but also over metrological events. The range of wind driven changes is dependent on estuary depth, wind velocity, and wind direction (Chen and Sanford 2009).

When the direct wind forcing stops, the estuary progresses to return to its tidal quasi steady state. This time period of restratification from episodic wind mixing events relative to typical conditions with dominant tidal mixing has been relatively understudied and is the focus of this paper. In stratified estuaries susceptible to wind mixing events, the changes in stratification have important implications for estuarine dynamics. Understanding the time scale that these indirect wind impacts occur is dependent on the estimation of the restratification time scale. Previous work by Li et al. (2007) examined a wind mixing event in Chesapeake Bay and observed restratification increased linearly with time reaching a quasi-steady state one day after the mixing event. This initial steady state failed to continue stratifying though and 5 days after the event the bay still could not reach pre-storm stratification levels.

Mobile Bay, a shallow highly stratified microtidal estuary, is an ideal system to examine the changes associated with wind mixing events. Changes in stratification can be large, and deviations from the tidal steady state can highlight important components of this restratification time period. The goal of this paper is to present observations of changes

in stratification after a bay-wide mixing event and highlight how the system evolves from being well-mixed back to a stratified estuary.

Data and Methods

Study Site

Mobile Bay is a shallow and wide estuary in the northern Gulf of Mexico. Like other estuaries in the northern gulf, the bay receives high river discharge. Mobile bay has relatively uniform bathymetry with an average depth of 3 m (Fig. 1). The exception to this is the deep (12-14 m) but narrow (120 m) ship channel that runs the length of the bay. The diurnal microtidal range fluctuates from <0.1 m during equatorial tides to 0.8 m during tropic tides. The high river discharge into the bay averages 1,516 $m^3 s^{-1}$ (Coogan and Dzwonkowski 2018) and varies throughout the year with low flow conditions in the summer. During the study period presented in this paper (July 2016) discharge averaged 313 $m^3 s^{-1}$, representative of average low flow summer conditions.

With its large river discharge and weak microtidal ranges, strong stratification is commonly observed throughout the bay (Schroeder et al. 1990; Ryan et al. 1997; Park et al. 2007; Dzwonkowski et al. 2011; Kim and Park 2012; Coogan and Dzwonkowski 2018). Noble et al. (1996) observed the system as being highly stratified (5 PSU m^{-1}), and resistant to mixing 80% of the time. These strong vertical salinity gradients are not easily broken down by the wind, but winter wind events can produce mixing power 6 to 8 times greater than the root mean square tidal current driven mixing (Schroeder et al. 1990). In summer, relatively calm winds allow stratification to persist for long periods of time until occasional strong summer storms mix the shallow water column. These changes in stratification from wind events can also lead to changes in estuary length with this system being highly responsive to mixing and changes in stratification (Coogan and Dzwonkowski 2018).

Observations

Three hydrographic boat surveys were conducted to observe the bay-wide spatial and temporal variability of salinity. The surveys were conducted on July 21, 28, and 30, 2016 with the first survey occurring before the mixing event on July 26-27, and the other two after the event. Each survey involved measuring vertical profiles with a Seabird SBE 25 in the channel and on the shoals of 5 transects (lines A-E in Fig. 1). The survey of all 5 lines took between 6-8 hours

106 to complete (1/3-1/4 of one diurnal tidal cycle). A total of 172 vertical profiles were collected to provide excellent
107 spatial observations throughout the bay.

108 Time-series data were collected at 4 mooring stations (stations MB, DI, MP, and CN in Fig. 1). Stations DI and
109 MP measured fixed near bottom salinity with YSI 6600s, which were used to calculate the along estuary density
110 gradient. Data were collected at 30-min frequencies and a low pass 48-hour Lanczos filter was used to isolate the
111 subtidal components. Station MB collected vertical profile data at 0.5 m intervals throughout the water column every
112 hour. Stations MB, DI, and MP are part of a long-term monitoring program through the Alabama Real-Time Coastal
113 Observation System, and in addition to the summer 2016 data, 10 years of data from 2006 to 2016 were used to analyze
114 long-term trends of restratification events. The last station CN collected data for 14 days from July 19 to August 2,
115 2016 and consisted of a near surface and near bottom YSI collecting 20-min data and 2 ADVs to collect near bottom
116 turbulence data. The ADVs were mounted horizontally and oriented perpendicular to the mean flow. Both ADVs had
117 a sampling rate of 16 Hz but used two different burst modes. The ADV 0.5 m off the bottom collected a 15-min burst
118 every hour, and the ADV 0.25 m off the bottom collected a 18-min burst every 2 hours. For quality control, ADV data
119 were discarded when velocity spikes exceeded 1 cm s^{-1}, signal to noise was less than 15 or correlation was less than
120 40. Large segments of poor data, 2 to 60 s in length, thought to be associated with fish contamination near the end of
121 the study period, were replaced by white noise scaled to the ensemble velocity variance following Davis and
122 Monismith (2011). Since the ADVs were mounted horizontally, periods when the mean flow was across estuary and
123 impacted by the instrument mounting were not included in the analyzed data set.

124 Daily river discharge data were obtained at two USGS gauging stations: the Claiborne L&D (USGS station
125 02428401) on the Alabama River and Coffeeville L&D (USGS station 02469762) on the Tombigbee River stations.
126 Both stations are roughly 130 km upriver from Mobile Bay. The combined river flow of the two stations was used as
127 the total river discharge into Mobile Bay, following Park et al. (2007).

128

129 **Analysis**

130 Turbulence was analyzed from the ADV data and used to estimate turbulent dissipation based on the inertial subrange
131 dissipation following the method in recent studies (Davis and Monismith 2011; Holleman et al. 2016; Huang et al.
132 2018). This was done by fitting the measured vertical velocity spectrum to a theoretical Kolmogorov -5/3 slope:

133 $$S(k) = \alpha \varepsilon^{2/3} k^{-5/3} \quad (4)$$

where S is the measured spectrum, k is the wavenumber, ε is turbulent dissipation, and α is the Kolmogorov constant (0.68). The frequency spectrum from the ADV was transformed to wavenumber space using Taylors frozen turbulence hypothesis. Figure 2 highlights the limits of the Kolmogorov fits for 2 spectral profiles in this study. The measured inertial subrange region of the frequency space was limited by the ADV sampling frequency at 16 Hz and the master turbulent length scale set by the Ozmidov length scale, $Lo = (\varepsilon/N^3)^{1/2}$ where N is the buoyancy frequency measured by the YSIs at station CN or the bottom boundary layer, $L_{BL} = \kappa z\sqrt{1 - z/h_{bl}}$ where $h_{bl}$is the height of the bottom boundary layer with the smaller of the two chosen for the master turbulent length scale, and ε was then solved iteratively. The ADV noise floor also limited the observed inertial subrange due to the ADV being mounted horizontally, thereby increasing the noise variance for the vertical velocity component (Voulgaris and Trowbridge 1998). Calculations of dissipation were also limited to periods when the burst average velocities were greater than 4 cm s^{-1} and periods when wave heights were less than 8 cm. Wave heights were estimated from linear wave theory and pressure measurements from the ADVs. The resulting data set provided estimates of turbulent dissipation that could be compared before and after the mixing event to examine the changes in turbulent characteristics occurring in the estuary.

To further understand the dissipation measurements, data were compared with a theoretical fit that estimates shear production from the bottom boundary layer balanced by dissipation for unstratified flows. The turbulent dissipation can then be set equal to shear production:

$$\varepsilon = \frac{U_{*b}^3}{\kappa z} \tag{5}$$

where κ is the von Karman constant (0.4) and z is distance off the bottom. This method has been used in previous studies (Jones and Monismith 2008; Davis and Monismith 2011) to highlight the deviation and influence of shear production from surface and internal waves and was used in this study to highlight the influence of stratification. Deviations from this production-dissipation balance can also be a result of divergences in the vertical flux of turbulence kinetic energy (TKE) and lead to observed dissipation values greater than the shear production in the outer bottom boundary layer (BBL) (Scully et al. 2011). To account for this, the method assumes that during unstratified periods in Mobile Bay the ADVs at 0.25 and 0.5 m are both in the inner log layer. Observations from another shallow (3.5 m) region of Mobile Bay by Ha and Park (2012) defined the BBL as 0.5 to 1.0 m off the bottom, though relatively strong currents can extend down to the near bed layer. This method provided a simple theory to examine the changes

occurring over the stratified to mixed periods and the assumption associated with this method is further expanded in the discussion.

In addition to the turbulent dissipation, the ADVs were used to quantify other aspects of the near bottom turbulent flow field including eddy viscosity (A_z), which was calculated by:

$$\overline{u'w'} = A_v \frac{\partial u}{\partial z} \tag{6}$$

where u' and w' are the fluctuating near bed velocities measured with the ADVs. The ADV data were also analyzed following the spectral model proposed by Kaimal et al (1972). The semi-empirical model based on atmospheric boundary layer data has a universal fit for normalized velocity autospectra data given as

$$\frac{kS(k)}{\overline{\beta'^2}} = \frac{0.16\frac{k}{k_o}}{1+0.16\left(\frac{k}{k_o}\right)^{5/3}} \tag{7}$$

where k_o is the intercept of the extrapolated inertial subrange spectrum and $\overline{\beta'^2}$ is the vertical velocity variance.

Tidal velocity was estimated based on continuity and the tidal volume changes in time. Similar methods were used by Coogan and Dzwonkowski (2018) for subtidal observations in Mobile Bay. The continuity estimates of tidal velocity were then used to calculate the friction velocity, U_{*b}, based on a quadratic drag stress, $U_{*b} = \sqrt{C_d}u_t$, where $u_t$is the tidal velocity and the bottom the drag coefficient, C_d, was calculated based on bottom stress measurements from the ADVs. The bottom stress was estimated as the near bed Reynolds stress, $\tau = \rho(-u'w')$. A limitation and source of errors associated with this method occurs when the sensors are outside the constant stress layer (Kim et al. 2000), and the 0.25 m sensor was assumed to be in the constant stress layer in this study. This continuity-based estimate of velocity allowed for an independent measure of theoretical turbulent dissipation to be calculated. The surface stress was estimated as

$$\tau_s = \rho_a C_{dw} W|W| \tag{8}$$

where ρ_a is the density of air, C_{dw} is the drag coefficient (0.0013), and W is the wind velocity.

Numerical Model

To evaluate changes in the residual velocity structure after a mixing event, the General Ocean Turbulence Model (GOTM) was used. The GOTM is a one-dimensional numerical model that solves the momentum, salt and heat transport equations with the latest turbulence closure models (Umlauf and Burchard 2005). This model has been

widely used in estuaries to evaluate changes in residual circulation, and the impact of stratification (Ralston and Stacey 2006; Burchard and Hofmeister 2008; Burchard 2009). For the model used in this study, the parameters representative of Mobile Bay, depth of 5 m and diurnal (24-hour) 0.15 m s^{-1} tidal velocity, were implemented and a $k-\varepsilon$ closure (Rodi 1987) with the stability constants from Canuto et al. (2001) were used.

The model was run for 14 tidal cycles before a mixing event was prescribed using an instantaneous 0.05 m s^{-1} vertical velocity. The model was then run until stratification returned and resulting residual velocities were calculated following Burchard and Hetland (2010) as the absolute value of the residual velocity profile,

$$\mathrm{M}(\langle u \rangle) = \frac{1}{H}\int_{-H}^{0} |\langle u(z) \rangle| dz \tag{9}$$

where $\langle u \rangle$ is the tidally averaged velocity. The velocities were then analyzed for the total residual velocity and its two components of the tidal straining and the combined gravitational and river discharge defined by Burchard and Hetland (2010) as

$$\langle u \rangle = \int_{-H}^{z} \frac{\langle A_v' \partial_z u' \rangle}{\langle A_v \rangle} d\xi + \frac{\partial_x b}{2}\int_{-H}^{z} \frac{\xi^2}{\langle A_v \rangle} d\xi + \langle p_x \rangle \int_{-H}^{z} \frac{\xi}{\langle A_v \rangle} d\xi \tag{10}$$

where the prime ($'$) denotes the tidally varying components, $\partial_x b$ is the along estuary buoyancy gradient, and p_x is the along estuary pressure gradient. In Eq. (10), the total residual velocity (L.H.S.) consists of three components: the tidal straining component (the first term on the R.H.S), the gravitational component (the second term) and the river discharge component (the third term).

Results

Stratification

In July 2016, a period of strong persistent stratification was broken down following a strong wind event in this shallow estuary where 73% of the bay is less than 4 m deep. The breakdown of stratification was due to a combination of wind stress, waves, and turnover in the bay. The mixing event began on July 24 when the surface salinity at station MB began increasing (Fig. 3a). This increase in surface salinity was a result of decreasing river discharge and a relatively steady 5 m s^{-1} westward wind (Fig. 3c). The westward winds can drive across-estuary setup that mixes the water column on the edges of the estuary, tilt isopycnals, and can turn the bay over if strong winds persist long enough. On July 25, the wind velocity increased up to 10 m s^{-1} and changed direction towards the northwest. This direction change resulted in a longer fetch for the bay increasing the wave height. The max significant wave height observed at station

CN was 0.4m. Unpublished historic wave data collected at station MB have an average wave height of 0.9 m corresponding with 10 m s^{-1} winds, and average summer significant wave height of 0.3 m. This change in wind direction and increased velocity further reduced the stratification observed at station MB to a minimum value of 1.3 PSU m^{-1}. The wind velocity then peaked on July 26 with a maximum speed of 15.1 m s^{-1} and further reduced the vertical stratification to 0 at station MB. The wind event was strong enough to completely mix the water column throughout the bay (with the exception of the deep ship channel). The average wind stress estimates during this 3-day period based on Eq. 8 was 0.06 Pa and had a maximum value of 0.36 Pa, but it should be noted these estimates did not include the effects of setup and setdown. In comparison to the estimated bottom stress from tidal velocities of 0.11 Pa during this same period. Reynolds stress measurements made with the ADV at 0.25 m had an average Reynolds stress of 0.15 Pa during the storm and peaked at 0.84 Pa. By comparison, the average Reynolds stress during the entire deployment of 0.07 Pa. The ADVs measured relatively small stresses on July 25 due to the westward component of the wind limiting the site's exposure to waves. On July 26 when the wind shifted towards the northeast Reynolds stress measurements increased.

This change in stratification was observed at the central site MB, where prior to mixing stratification reached a depth average 4.4 PSU m^{-1} (Fig. 3a) and was as high as 20.6 PSU m^{-1} in the pycnocline. The strong stratification was observed bay wide on July 21 from the CTD transect data and can be seen at the northernmost (line A) and southernmost (line E) transect lines (Fig. 4). Depth average salinity gradients during this survey ranged from 5.0 to 0.5 PSU m^{-1}. The stratification was concentrated over a sharp pycnocline (2.2 m from the surface) where gradients reached as high as 20 PSU m^{-1} on all the transect lines (lines A-E). This period of strong stratification had persisted over the previous 16 days with some tidal variability (Fig. 3a). When winds at station MB relaxed on July 27, a quick return of a salinity gradient of 4.7 PSU over the water column occurred (Fig. 3a). This initial return slowed in the following days as the vertical salinity gradient grew at every tidal cycle and showed large tidal variability. Stratification reached a maximum depth average of 2.5 PSU m^{-1} and gradient maximum of 12.2 PSU m^{-1} on July 31 (4 days after the event) but was still far weaker than the pre-mixing event level.

CTD transects showed similar trends of moderate increases in stratification one and three days after the mixing event (Fig. 4). One day after the mixing event (July 28) the average stratification ranged from 2.8 to 0 PSU m^{-1} and had a bay-wide average 0.8 PSU m^{-1}. Three days after the mixing event (July 30) the stratification ranged from 2.3 to 0 PSU m^{-1} and had a bay-wide average of 1.1 PSU m^{-1}. This moderate increase was not uniform across the estuary.

Stations nearest the mouth showed stronger stratification relative to the up-estuary stations. In Fig. 5, the 10 strongest (red dots) and 10 weakest (blue dots) stratified sites are shown based on the CTD surveys. On July 21 (before mixing) no clear pattern existed in the locations of strong and weak stratification. On July 28 (1 day after the mixing event), the most stratified sites are the 10 closest to the estuary mouth, and the least stratified sites occurred in the shallower and inner regions of the bay. Three days after the event on July 30, the same pattern was observed but with returning stratification propagating up estuary.

This return in stratification can also be seen in the cross-estuary plots (Fig. 4) where the northernmost line (A) showed very little return in stratification on July 28 and 30 compared to the southernmost line (E). It is interesting to note the spatial variability in the cross-bay direction is less uniform after the mixing. Prior to the mixing event a well-developed sharp pycnocline was observed across the estuary, and after mixing a broader spatially varying pycnocline was formed as stratification was returning. The southernmost line (E) showed faster returns in stratification but was also spatially variable in the cross-estuary direction and was made up of a relatively broad pycnocline over the water column.

Turbulence

Data from two ADVs at station CN (0.25 and 0.5 m above the seafloor) showed similar ranges in dissipation. Useable data were limited by wave free days. Poor fits of data to the -5/3 slope and values of the inertial sub-range falling below the ADV sampling rate limited dissipation measurements 22% of the time during wave free periods. It should be noted that during the stratified period, higher levels of local stratification existed in the water column, but analysis and calculation of L_o was limited by the availability of the near surface and near bottom YSI observations. Estimates of dissipation for the two ADVs averaged $2.6{-}3.1 \times 10^{-5}$ m^2 s^{-3} prior to the mixing event and increased to $1.4{-}8.5 \times 10^{-4}$ m^2 s^{-3} after the mixing event, indicating increasing turbulence dissipation with decreasing stratification. When the buoyancy frequency was greater than 0.1 s^{-1} dissipation values fell below 10^{-4} m^2 s^{-3}. This stratification value of 0.1 s^{-1} is of note because prior to mixing stratification stayed above 0.1 s^{-1} and after mixing returning stratification stayed below 0.1 s^{-1}.

The vertical turbulent length scale was estimated based on fitting the vertical velocity autospectra from the ADV data to the Kaimal spectrum (Kaimal et al. 1972). Two periods were focused on, a flood tide before the mixing event on July 21 and a flood tide after the mixing event on July 30 (Fig. 6). On July 21 when stratification was strong the

normalized autospectra failed to capture the semi-empirical Kaimal spectrum, highlighting the limits of capturing low dissipation values at both 0.25 m and 0.50 m due to the noise floor of the ADV covering a large portion of the inertial subrange. The autospectra is also closely bound on either side by the internal wave energy and the high noise floor limiting comparisons with the Kaimal model. Nine days later after the mixing event the autospectra showed an improved fit with the Kaimal spectrum where k_o values were in line with the estimated bottom boundary layer length scales.

To further understand the role of stratification, measurements of dissipation were compared with a theoretical fit. Figure 7 shows the relationship of the observed dissipation over the theoretical bottom boundary layer shear production, where values less than 1 suggest turbulence was being suppressed, values equal to one match the theory, and values greater than one indicate turbulent production was occurring outside the bottom boundary layer. When plotted against stratification a general pattern of increasing variability with increasing stratification can be observed. The bulk of this transition occurred around 0.1 s^{-1}, before and after the mixing event. The pattern shows that, as expected, under low stratification, Eq. 5 provides a reasonable fit for the balance of shear production and turbulent dissipation. As stratification increased though, turbulent production and turbulent suppression were both observed to increase in the estuary.

To understand the periods of increasing variability from the theoretical fit, the ADV burst average velocities were plotted for both ADVs (Fig. 8a). The times when estimated shear production from the bottom boundary layer was larger than turbulence dissipation ($\varepsilon\kappa z/u^3_{*b} < 1$) can be observed occurring at peak ebb and flood tides. This was when the velocity profile was fully developed, and the bottom shear production was large enough to interact with the overlying stratification. The strong stratification can be seen in Fig. 8b where at peak flood (yellow profile) there was a large near bottom mixed layer and strong overlying stratification. Six hours later at the end of flood (purple profile) there was still strong depth average stratification, but the overall stratification had been broken down by internal shear. It was also observed that prior to the mixing event (July 26) the stratified period had a large number of black dots (turbulent suppression) occurring on both peak ebb and flood tides. After the mixing event though, there were three tidal cycles where black dots occurred only on the ebb tide. Salinity profiles in Fig. 8b during this time show well mixed condition (green profile) were observed during ebb tide one day after the mixing event. Seven hours later a small increase in stratification was observed (light blue profile) at the end of the ebb tide that coincided with a period of $\varepsilon\kappa z/u^3_{*b} < 1$. Three days after the mixing event at the end of flood a well-mixed salinity profile was observed (maroon

profile). This asymmetry in turbulence and stratification suggested tidal asymmetry was important after the mixing event during these three tidal cycles. After August 1 (5 days after the mixing event) the occurrence of turbulent suppression (black dots) began to increase on both ebb and flood tides.

Evidence of tidal straining was also observed from the calculated eddy viscosity. During flood tides when stratification was less than 0.1 s^{-1} (after the mixing event), the average eddy viscosity was $5.5x10^{-3}$ m^2s^{-1} with a standard deviation of $8.3x10^{-3}$. On ebb tides during this same period of low stratification the eddy viscosity was smaller with an average value of $9.8x10^{-4}$ m^2s^{-1} and a standard deviation of $1.1x10^{-3}$. This change in eddy viscosity between ebb and flood tides can drive subtidal changes in circulation.

Residual Circulation

With the appearance of tidal asymmetry in the turbulence data and eddy viscosity but with the limited field measurements to quantify the impact of tidal straining, the 1D GOTM was used to examine the changes in residual circulation associated with the mixing event. Figure 9 shows model results for the mean absolute exchange velocities for the total residual exchange and its two components of the tidal straining and the combined gravitational and river discharge. The results show that for the first two tidal cycles after the mixing event the strain and gravitational components are nearly balanced. Around the third tidal cycle after the mixing event the tidal strain component peaks, while the gravitational and depth average stratification continues to increase. These results show that in stratified systems gravitational exchange is the dominant process while stratified, but during periods of returning stratification after a mixing event there is a change in the relative contribution between the two components.

Discussion

Restratification timescale

Observations and model results show wind mixing events can cause large changes in estuary stratification that impact both turbulence and the residual velocity. A quick initial return in stratification was followed by a continuous yet slow increase in stratification over the next five days (Fig. 3a). This return peaked at a depth averaged 2.5 PSU m^{-1} and was a little over half the initial stratification before the mixing event. The timeseries and spatial data suggest there were 2 regimes of returning stratification: an initial rapid return associated with straining of the density gradient and a subsequent slower restratification dependent on the removal of mixed water and limited by exchange and mixing.

Simpson and Linden (1989) demonstrated through laboratory experiments the changes and timescales of gravitational adjustment for fluids under constant and non-constant horizontal gradients. The non-constant gradients resulted in frontogenesis driving the gravitational adjustment, and constant gradients resulted in an increase of stratification with an analytical solution of

$$N^2 = Ri(\beta g t)^2 \left(\frac{\partial s}{\partial x}\right)^2 \quad (11)$$

where *Ri* is the Richardson number (0.5). This analytical solution states that the increase in buoyancy frequency is due to the tilt of the along-estuary density gradient and increases as a function of the salinity gradient and time. Solving this equation provides an estimate of 20 hours for the stratification to return to the pre-event levels. This quick return in restratification from the along-estuary gradient likely sets up the initial rapid return (Fig. 3), but the high stratification levels observed before the mixing event are limited by subtidal exchange and mixing not accounted for in Eq. 11.

This fast response in restratification was observed to be most pronounced near the bay mouth (Fig. 5). Tidal fronts are common in this area and likely enhance local density gradients, resulting in the fast restratification observed near the mouth. The localized increase in the density gradient is thought to lead to frontogenesis near the mouth. Geyer and Ralston (2015) examined frontogenesis in the Hudson River observing the fronts propagating landward through the estuary and suggested that they may be an essential component of the spring-to-neap transition for restratification. The bay-wide observations showed that after a mixing event there was a non-uniform return in stratification (Fig. 4). Through the development of localized fronts around the areas of increased density gradients, the hotspots of restratification can develop after mixing events. The non-uniform return in stratification was also observed by Li et al. (2007) in Chesapeake Bay, where the stratification was spatially variable in the days following a wind mixing event from a hurricane. These hotspots are not only a source of restratification but also likely causing spatial variability in sediment transport and biogeochemical processes in the bay.

The second phase of restratification is dependent on the removal of mixed water and limited by residual circulation and mixing. This slow return requires the water mixed by the wind be replaced with low and high salinity water to redevelop the strong vertical gradients that used to exist before the mixing event. This can be seen at station MB where the salinities were 26 and 12 PSU at the bottom and surface, respectively, before the mixing event (Fig. 3a). After the mixing event the northernmost line A (10.6 km northward of station MB) has a trace amount of water with 12 PSU salinity and the southernmost line E (12.1 km southward of station MB) has a trace amount of water with 26 PSU (Fig.

4). This limits the vertical salinity gradient that can develop until this portion of the bay circulates new high and low salinity water through it.

This second phase of replacement of mixed water and returning stratification can be solved in terms of a salinity variance budget following MacCready et al. (2018)

$$\frac{d}{dt}\int s'^2\, dV = -\int u_n\, s'^2 dA_{open} - 2\int K_z(\nabla s')^2 dV \quad (12)$$

where V is the volume, s' is the salinity variance (the deviation from the volume averaged salinity) and u_n is the outward normal velocity through the boundary with area A_{open}. Equation 12 states that the rate of change in net salinity variance (L.H.S.) is governed by advective input/output of salinity variance from exchange and river discharge (1st term on the R.H.S.) and a loss from mixing (2nd term R.H.S.). Changes in salinity variance were solved based on the CTD bay-wide transect data. When the observed returning stratification on July 28 was compared to the condition on July 21, a 2.63×10^{10} $(g/kg)^2$ m^3 loss of variance was estimated over the 5-day period (and the bulk of the loss was likely concentrated over the 2-day wind event). Comparison of July 28 to July 30 showed a 1.3×10^4 $(g/kg)^2$ m^3 s^{-1} rate of return in variance. With this rate of return, it would take 22.5 days for the bay to return to the pre-mixing state (the loss from July 21-28). This slower return is limited by exchange and mixing, and the estimated 22.5 days of restratification time was likely to decrease as stratification increased, which would have enhanced circulation and limited mixing.

These changes in circulation associated with increasing stratification can drive a nonlinear return in stratification time. The GOTM model used in this study showed the importance of tidal straining in driving initial subtidal exchange velocities. As the stratification increases, the circulation dynamics transitions in such a way that gravitational exchange dominates subtidal velocity. Future work should focus on the relative contribution of tidal straining, river discharge, and gravitational exchange in the salinity variance to further identify the importance of these processes on the restratification timescales.

To understand restratification beyond the one event on July 26-27, 2016, the long-term data at station MB (2006-2016) were used to estimate restratification times in the bay for a total of 178 mixing events. The time scale was estimated based on the time it took a mixed water column (vertical gradient less than 0.2 PSU m^{-1}) to return to a 2.8 PSU m^{-1} level of stratification (the average stratification at station MB when winds are less than 5 m s^{-1}). The average return in stratification took 2.3 days with a standard deviation of 1.8 days. These estimates are comparable to that for the event in July 2016 at station MB, but much shorter than the estimate based on salinity variance. This is likely due

to the fact that one is based on the data at one point (located on the edge of the ship channel) whereas the other is based on the bay-wide data.

With the long-term data, river discharge was noted as having a large impact on the restratification time scale (Fig. 10). Two general trends were noted that increasing river discharge not only decreases the restratification time but also reduces its variability. Efforts were made to further determine the forcing conditions driving the increased variability, but no significant trends could be determined from wind direction, duration, or magnitude. The only qualitative trend observed was due to the level of stratification in Mobile Bay that was present before the mixing event. Previous work in Mobile Bay has highlighted that up/down-estuary winds can significantly enhance/inhibit exchange flow, and during periods of low discharge up-estuary winds can reverse the subtidal exchange and salt transport (Coogan and Dzwonkowski 2018). This subtidal along-estuary wind-exchange interaction under low discharge may play a role in the increased range of restratification times from 0 to >8 days. Li and Li (2011) also observed stratification took longer to recover after up-estuary wind but on the order of 1-3 weeks and this response may be magnified at low discharge. The varying response time at low discharge is likely due to several variables associated with the wind forcing conditions that drive the event, as well as pre-existing stratification condition in the bay prior to the mixing event. The faster restratification with increasing discharge is associated with increased estuarine exchange. Previous studies (Kim and Park 2012; Du et al. 2018) showed increasing net outflux/influx from/into Mobile Bay with increasing river discharge. The higher exchange flux (1st term on the R.H.S. of Eq. 12) would increase the rate at which outflux removed low variance (mixed water) from the bay and influx introduced the ocean water and river discharge that added variance to the estuary. Outliers of slow restratification at high discharge are associated with freshet events in the bay. During these times the river discharge values that peaked as high as 7500 $m^3 s^{-1}$ and fell to 1,000 $m^3 s^{-1}$ one week later resulting in unique forcing conditions driving the observed trends in the bay.

Turbulent Changes

The ADV timeseries captured changes from the stratified period through the return in stratification. The range of turbulent dissipation values observed in this study is comparable to other near bottom measurements from an up-estuary region of San Francisco Bay ($10^{-7} - 10^{-5}$ $m^2 s^{-3}$, Jones and Monismith 2008) and Hudson River estuary (10^{-7}–10^{-4} $m^2 s^{-3}$, Peters and Bokhorst 2000). Data in this study showed with increasing stratification turbulent dissipation decreased. This relationship between stratification and turbulence can be described with the buoyancy

Reynolds number, $Re_b = \varepsilon/(\nu N^2)$ where ν is kinematic viscosity (Gibson 1986; Holleman et al. 2016). Previous modeling work by Shih et al. (2005) suggested there are three regimes of mixing: energetic, transitional, and molecular, with $7 < Re_b < 100$ representing the transitional regime. The median Re_b in this study was 2700, but Re_b decreased to 850 during periods of inhibited shear production ($\varepsilon\kappa z/u^3_{*b} < 1$), and fell below 100 (into the transitional regime) 2% of the time. It should be noted that in this study Re_b was based on the underestimated N values calculated from near bottom and near surface data, which resulted in the overestimated Re_b values and the real values are likely smaller than those reported in this study.

For stratification to return after the mixing event there must be a vertical shear of the density gradient (2nd term on the L.H.S. of Eq. 2) that exceeds mixing (R.H.S. of Eq. 2). This initial return, as previously discussed, occurs through tidal straining and is also referred to as strain-induced periodic stratification in Simpson et al. (1990), where increased stratification at peak ebb decreases mixing (black dots only at peak ebb for 3 days after the mixing event in Fig. 8a) and decreased stratification allows for a fully developed bottom boundary layer at flood tide. This change leads to an asymmetry in the tidal momentum balance that creates a residual circulation (Burchard and Hetland 2010; Geyer and MacCready 2014). The asymmetries observed in this study persisted until stratification values were large enough to enhance the gravitational circulation via eddy viscosity and dominated the subtidal circulation.

Comparing the bottom boundary layer shear production estimates with observations of dissipation highlighted the importance of buoyancy flux on peak ebb and flood where the turbulent suppression was most active. These results are comparable to Stacey and Ralston (2005) where they observed the top of the bottom boundary layer is associated with relatively strong shear and stratification that can be described as a balance between strain-induced buoyancy flux and the production of turbulent energy. This means the assumption in Eq. 5 that dissipation is balanced by only shear production is not valid and is reflected by the less than one deviation at peak ebb and flood in this study. The limited salinity profiles from the ADV site also highlighted some tidal asymmetries, where the July 21 profile taken at peak flood (yellow profile in Fig. 8b) showed a well-mixed bottom boundary layer extending 1 m off the bottom. Stacey and Ralston (2005) observed similar well-mixed bottom boundary layers on flood tides with a height limited by the strain-induced buoyancy flux that switched from destabilizing to stabilizing. After the mixing event, flood tides without black dots occurred when this stabilizing buoyancy flux (maroon profile in Fig. 8b) was absent and shear production was balanced by dissipation.

Deviations in the production-dissipation balance can also occur during unstratified periods. Scully et al. (2011) observed dissipation exceeds production in the upper half of the boundary layer and is due to the vertical turbulent transport of TKE from the lower boundary layer. Though these mechanisms are likely impacting the observations in this study, trends highlighted in Figs. 7 and 8 were observed at both 0.25 m and 0.5 m off the bottom covering a large range of the near bottom profiles and the potential changes due to the vertical flux of TKE. The tidal asymmetries seen in this study are also not uncommon, Peters and Bokhorst (2000) observed asymmetries in dissipation between flood and ebb but their data showed an opposite trend of higher dissipation on ebb. This difference may reflect changes higher in the water column that were not observed in this study.

Not shown in Fig. 8a were points where $\varepsilon\kappa z/u^3_{*b} > 1$ when shear production exceeded estimates. These values occurred when tidal velocity was low and suggest shear instabilities higher in the water column are advecting turbulence downward or the Taylors frozen turbulence hypothesis is no longer valid at these low velocities. Scully et al. (2011) observed TKE diffusing away from regions of high shear production. This stress from the shear layer can be exported to regions of low shear and become coupled into the bottom boundary layer that would lead to periods of $\varepsilon\kappa z/u^3_{*b} > 1$. Extending turbulence measurements throughout the water column is needed in future work to further understand these values.

Estimates of log BBLs can be highly variable and sensitive to stratification (Kim et al. 2000). This variability makes the comparisons and assumptions in this study limited yet provides a strong foundation to compare the deviations around this sensitivity to changes occurring in Mobile Bay over tidal and subtidal time scales. Near bed suspended sediment concentrations were not measured in this study and can also impact BBL structure and stratification (Friedrichs et al. 2000). Previous work by Ha and Park (2012) in Mobile Bay observed that during periods of stratification the relative contribution of suspended sediment concentration to the density gradient is two orders of magnitude smaller than that of the thermohaline gradient and was assumed negligible in this study.

Conclusion

Observations from Mobile Bay showed that, after a mixing event, moderate increases in stratification occurred over 2-3 days and were spatially variable. Sites close to the estuary mouth had the earliest return in stratification and with each tidal intrusion from the ocean the stratification pushed inward into the bay. Salinity variance estimates based on the bay-wide data suggested that the restratification to the pre-mixing levels would take 22.5 days. This long return

period indicates that if strong wind events in Mobile Bay occur more often than every ~22.5 days the system may not have enough time to fully restratify and reach a tidal (wind free) quasi steady state condition. Long-term observations showed that river discharge can change this response time and the restratification timescale. Based on the observations, estimates of stratification in Mobile Bay can be scaled as a function of river discharge and wind mixing.

Changes in the occurrence of turbulent suppression associated with stratification was clearly observed in the time-series data, which provided insight on how returning stratification and circulation are changing after the mixing event. The model results further highlighted this change in relative contribution of tidal straining and gravitational exchange. These results have important implications for variables of interest after storm events, where the fate of suspended sediment stirred up after a storm event will be advected and deposited differently than under a stratified period.

Acknowledgements Long-term data were collected by the Tech Support Group at the Dauphin Island Sea Lab, including Kyle Weis, Roxanne Robertson, Alan Gunter, Mike Dardeau, G. Lockridge, Hunter King, Y. Hintz and L. Linn and R. Collini (Data available at www.mymobile.com). The authors would like to acknowledge Steve Dykstra, Kara Gadeken, Cy Clemo, Jacob Blandford, and Jenine Brideau for their help with field data collection. This research was made possible in part by NOAA Restore program (NA17NOS4510101), and the Center for Environmental Resiliency at University of South Alabama. We acknowledge comments provided by the two anonymous reviewers that helped to improve this manuscript.

References

Burchard H. 2009. Combined effects of wind, tide, and horizontal density gradients on stratification in estuaries and coastal Seas. *Journal of Physical Oceanography*. doi:10.1175/2009JPO4142.1

Burchard H, and Hetland R. 2010. Quantifying the contributions of tidal straining and gravitational circulation to residual circulation in periodically stratified tidal estuaries. *Journal of Physical Oceanography*. doi:10.1175/2010JPO4270.1

Burchard H, and Hofmeister R. 2008. A dynamic equation for the potential energy anomaly for analysing mixing and stratification in estuaries and coastal seas. *Estuarine, Coastal and Shelf Science*. doi:10.1016/j.ecss.2007.10.025

Canuto V, Howard A, Cheng Y, and Dubovikov M. 2001. Ocean turbulence. Part I: One-point closure model - momentum and heat vertical diffusivities. *Journal of Physical Oceanography*. doi:10.1175/1520-0485(2001)031<1413:OTPIOP>2.0.CO;2

Chen S, and Sanford L. 2009. Axial Wind Effects on Stratification and Longitudinal Salt Transport in an Idealized, Partially Mixed Estuary. *Journal of Physical Oceanography*. doi:10.1175/2009JPO4016.1

Coogan J, and Dzwonkowski B .2018. Observations of wind forcing effects on estuary length and salinity flux in a river-dominated, microtidal estuary, Mobile Bay, Alabama. *Journal of Physical Oceanography*. doi:10.1175/JPO-D-17-0249.1

Davis K, and Monismith S. 2011. The modification of bottom boundary layer turbulence and mixing by internal waves shoaling on a barrier reef. *Journal of Physical Oceanography*. doi:10.1175/2011JPO4344.1

Du J, Park K, Shen J, Dzwonkowski B, Yu X, and Yoon B. 2018. Role of baroclinic processes on flushing characteristics in a highly stratified estuarine system, Mobile Bay, Alabama. *Journal of Geophysical Research: Oceans*. doi:10.1029/2018JC013855

Dzwonkowski B, Park K, Ha H, Graham W, Hernandez F, and Powers S. 2011. Hydrographic variability on a coastal shelf directly influenced by estuarine outflow. *Continental Shelf Research*. doi:10.1016/j.csr.2011.03.001

Friedrichs C, Wright L, Hepworth D, and Kim S. 2000. Bottom-boundary-layer processes associated with fine sediment accumulation in coastal seas and bays. *Continental Shelf Research*. doi:10.3354/meps192219

Geyer W. 1993. The importance of suppression of turbulence by stratification on the estuarine turbidity maximum. *Estuaries*. doi:10.2307/1352769

Geyer W, and MacCready P. 2014. The estuarine circulation. *Annual Review of Fluid Mechanics*. doi:10.1146/annurev-fluid-010313-141302

Geyer W, and Ralston D. 2015. Estuarine frontogenesis. *Journal of Physical Oceanography*. doi:10.1175/JPO-D-14-0082.1

Geyer W, Trowbridge J, and Bowen M. 2000. The dynamics of a partially mixed estuary. *Journal of Physical Oceanography*. doi:10.1175/1520-0485(2000)030<2035:TDOAPM>2.0.CO;2

Gibson C. 1986. Internal waves, fossil turbulence, and composite ocean microstructure spectra. *Journal of Fluid Mechanics*. doi:10.1017/S0022112086000307

Ha H, and Park K. 2012. High-resolution comparison of sediment dynamics under different forcing conditions in the bottom boundary layer of a shallow, micro-tidal estuary. *Journal of Geophysical Research: Oceans*. doi:10.1029/2012JC007878

Hansen D, and Rattray M. 1966. Gravitational circulation in straits and estuaries. *Journal of Marine Research*. 23:104:122.

Holleman R, Geyer W, and Ralston D. 2016. Stratified turbulence and mixing efficiency in a salt wedge estuary. *Journal of Physical Oceanography*. doi:10.1175/JPO-D-15-0193.1

Huang C, Ma H, Guo J, Dai D, and Qiao F. 2018. Calculation of turbulent dissipation rate with acoustic Doppler velocimeter: Calculation of turbulent dissipation rate. *Limnology and Oceanography: Methods*. doi:10.1002/lom3.10243

Jones N, and Monismith S. 2008. The influence of whitecapping waves on the vertical structure of turbulence in a shallow estuarine embayment. *Journal of Physical Oceanography*. doi:10.1175/2007JPO3766.1

Kaimal, J. C., Wyngaard, J. C. J., Izumi, Y., and Coté, O. R. 1972. Spectral characteristics of surface-layer turbulence. *Quarterly Journal of the Royal Meteorological Society*. *98* (417), 563-589.

Kim S, Friedrichs C, Maa J, and Wright L. 2000. Estimating bottom stress in tidal boundary layer from acoustic Doppler velocimeter data. *Journal of Hydraulic Engineering*. doi:10.1061/(ASCE)0733-9429(2000)126:6(399)

Kim C, and Park K. 2012. A modeling study of water and salt exchange for a microtidal, stratified northern Gulf of Mexico estuary. *Journal of Marine Systems*. doi:10.1016/j.jmarsys.2012.02.008

Li M, Zhong L, Boicourt WC, Zhang S, and Zhang DL. 2007. Hurricane-induced destratification and restratification in a partially-mixed estuary. *Journal of Marine Research*. doi:10.1357/002224007780882550

Li Y, and Li M. 2011. Effects of winds on stratification and circulation in a partially mixed estuary. *Journal of Geophysical Research*. doi:10.1029/2010JC006893

MacCready P, and Geyer W. 2010. Advances in estuarine physics. *Annual Review of Marine Science*. doi:10.1146/annurev-marine-120308-081015

MacCready P, Geyer W, and Burchard H. 2018. Estuarine exchange flow is related to mixing through the salinity variance budget. *Journal of Physical Oceanography*. doi:10.1175/JPO-D-17-0266.1

Noble M, Schroeder W, Wiseman W, Ryan H, and Gelfenbaum G. 1996.Subtidal circulation patterns in a shallow, highly stratified estuary: Mobile Bay, Alabama. *Journal of Geophysical Research*. doi:10.1029/96JC02506.

Park K, Kim C, and Schroeder W. 2007. Temporal variability in summertime bottom hypoxia in shallow areas of Mobile Bay, Alabama. *Estuaries and Coasts.* doi:10.1007/BF02782967

Peters H, and Bokhorst R. 2000. Microstructure observations of turbulent mixing in a partially mixed estuary. Part I: Dissipation rate. *Journal of Physical Oceanography*. doi:10.1175/15200485(2000)030<1232:MOOTMI>2.0. CO;2

Pritchard D. 1956. The dynamic structure of a coastal plain estuary. *Journal of Marine Research*. 15(1):33–42.

Ralston D, and Stacey M. 2006. Shear and turbulence production across subtidal channels. *Journal of Marine Research*. doi:10.1357/002224006776412359

Rodi W. 1987. Examples of calculation methods for flow and mixing in stratified fluids. *Journal of Geophysical Research: Oceans*. doi:10.1029/JC092iC05p05305

Ryan H, Noble M, Williams E, Schroeder W, Pennock J, and Gelfenbaum G. 1997. Tidal current shear in a broad, shallow, river-dominated estuary. *Continental Shelf Research*. doi:10.1016/S0278-4343(96)00053-2

Schroeder W, Dinnel S, and Wiseman W. 1990. Salinity stratification in a river dominated Estuary. *Estuaries*. doi:10.2307/1351583

Scully M, Geyer W, and Trowbridge J. 2011. The influence of stratification and nonlocal turbulent production on estuarine turbulence: An assessment of turbulence closure with field observations. *Journal of Physical Oceanography*. doi:10.1175/2010JPO4470.1

Shih L, Koseff J, Ivey G, and Ferziger J. 2005. Parameterization of turbulent fluxes and scales using homogeneous sheared stably stratified turbulence simulations. *Journal of Fluid Mechanics*. doi:10.1017/S0022112004002587

Simpson J, and Linden P. 1989. Frontogenesis in a fluid with horizontal density gradients. *Journal of Fluid Mechanics*. doi:10.1017/S0022112089001072

Simpson J, Brown J, Matthews J, and Allen G. 1990. Tidal straining, density currents, and stirring in the control of estuarine stratification. *Estuaries*. doi:10.2307/1351581

Stacey MT, Ralston DK. 2005. The scaling and structure of the estuarine bottom boundary layer. *Journal of Physical Oceanography*. doi:10.1175/JPO-2672.1

Stacey M, Burau J, and Monismith S. 2001. Creation of residual flows in a partially stratified estuary. *Journal of Geophysical Research: Oceans*. doi:10.1029/2000JC000576

Umlauf L, and Burchard H. 2005. Second-order turbulence closure models for geophysical boundary layers. A review of recent work. *Continental Shelf Research*. doi:10.1016/j.csr.2004.08.004

Voulgaris, G. and Trowbridge, J.H. 1998. Evaluation of the acoustic Doppler velocimeter (ADV) for turbulence measurements. *Journal of atmospheric and oceanic technology*. doi:10.1175/1520-0426(1998)015<0272:EOT ADV>2.0.CO;2

Valle-Levinson A. 2010. Definition and classification of estuaries. In: Contemporary Issues in Estuarine Physics, ed. A. Valle-Levinson, 1-11. New York: Cambridge University Press.

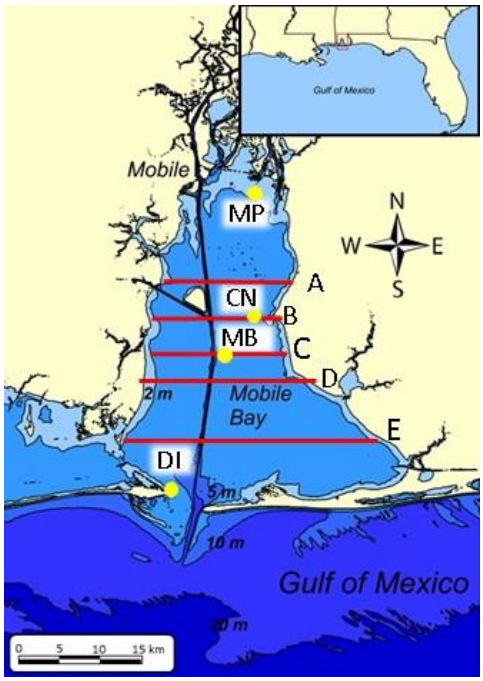

Fig. 1 Map of study site, Mobile Bay, located in the northern Gulf of Mexico, showing the CTD survey lines on July 21, 28 and 30, 2016 (red lines) and the time series stations (yellow dots).

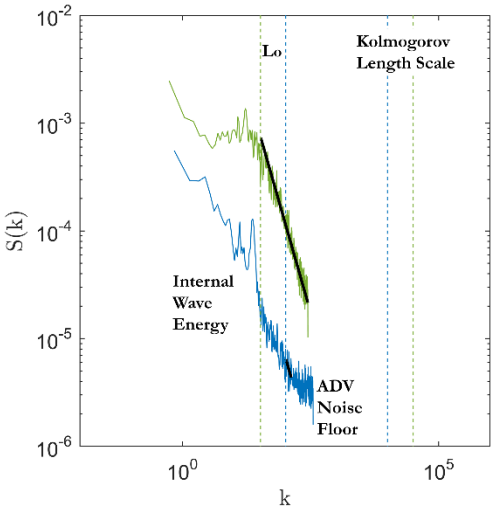

Fig. 2 Example of vertical velocity spectrum for 2 ADV burst at 8:17 on July 21 during the highly stratified period (blue) and 00:17 on July 30 after the mixing event (green). The inertial subrange is limited by the master turbulent length scale and the Kolmogorov length scale.

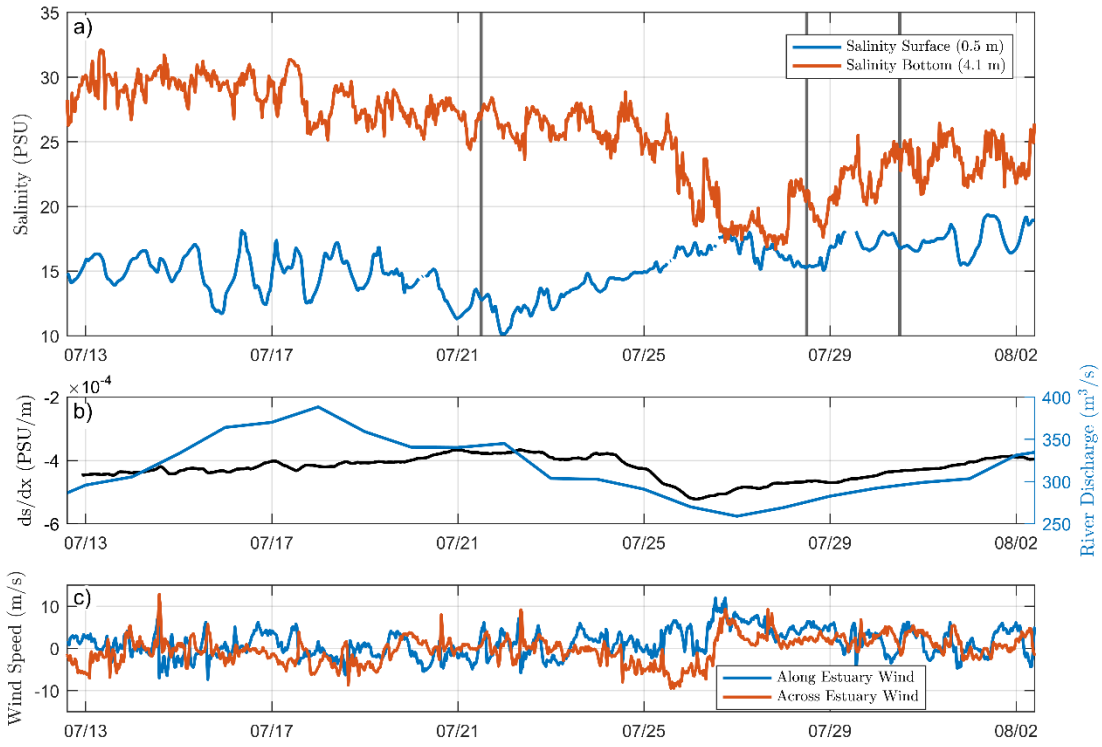

602

603 **Fig. 3** Time series data from Station MB for (a) the surface (0.5 m from surface) and bottom (4.1 m from surface)
604 salinity, with the vertical lines denoting CTD survey dates, (b) the along-estuary salinity gradient between stations
605 MP and DI, and river discharge into Mobile Bay and (c) the hourly wind speed components along (positive north
606 direction of travel) and across (positive east direction of travel) the bay.

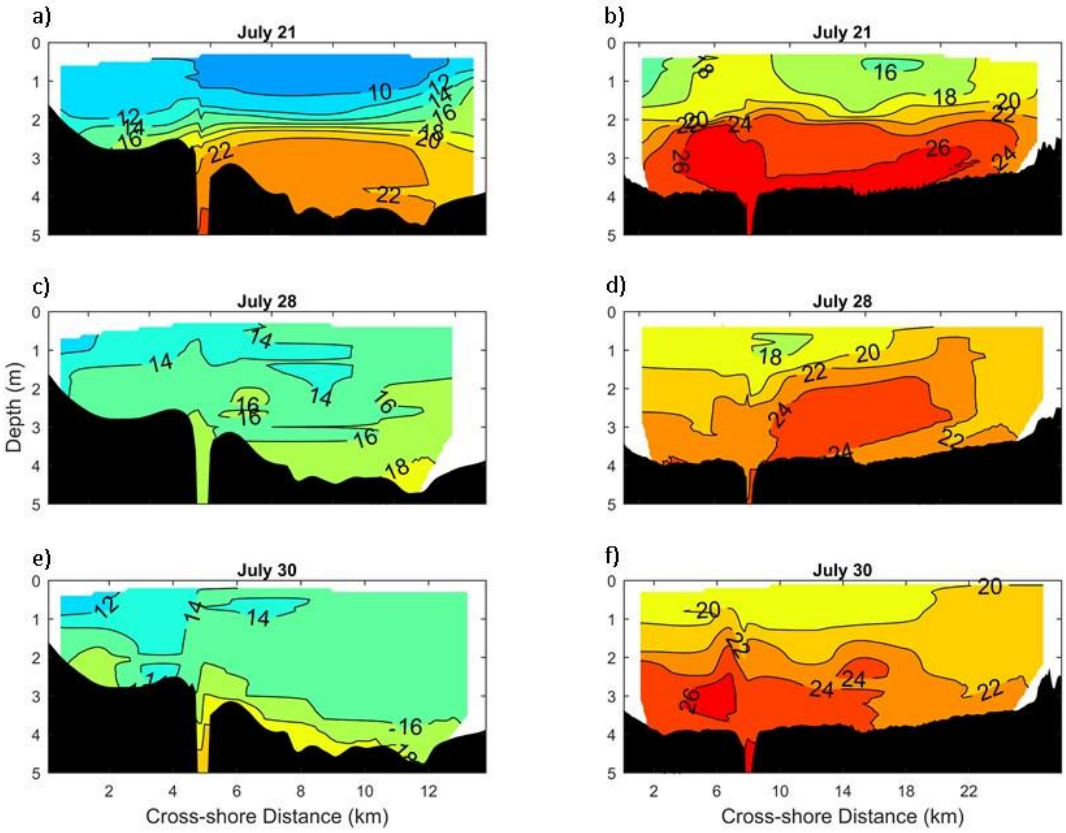

608 **Fig. 4** Profiles of salinity at transects A (a,c,e) and E (b,d,f) where July 21 is before the mixing event and July 28 and
609 30 are one and three days after the mixing event, respectively. Profiles are shown only for the top 5 m, although the
610 narrow deep ship channel is 12-14 m deep.
611

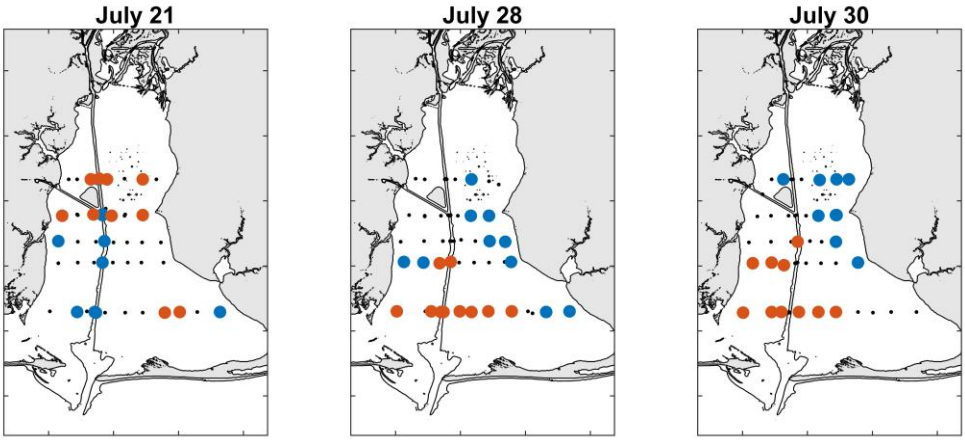

Fig. 5 Spatial data from the CTD casts showing the locations of vertical profiles with the 10 strongest (red dots) and 10 weakest (blue dots) stratification.

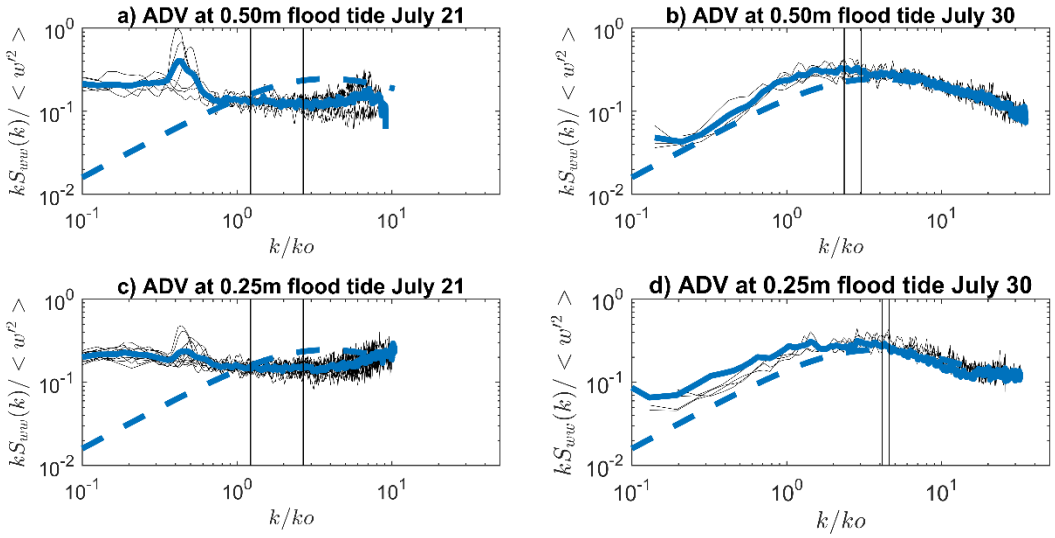

Fig. 6 Normalized vertical velocity autospectra at 0.5 m above the bottom during a flood tide on (a) July 21 and (b) July 30, and 0.25 m above the bottom during a flood tide on (c) July 21 and (d) July 30. Black lines show individual auto spectra, the solid blue lines are bin averaged data, and the dashed blue lines are the nondimensional spectra of Kaimal et al. (1972). Vertical black lines denote the predicted master turbulent length scale based on bottom boundary layer scaling (b,d) and Ozimidov scaling (a,c). July 21 and 30 are before and after the mixing event, respectively.

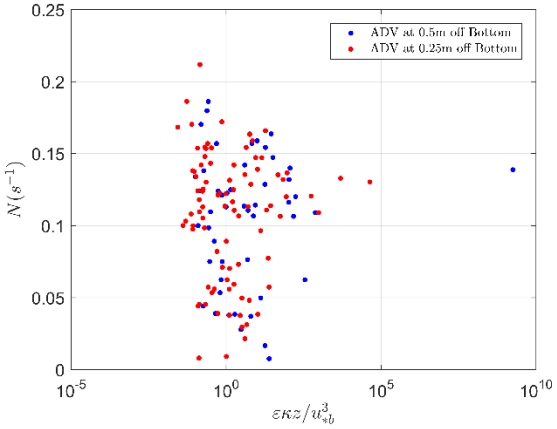

Fig. 7 Observed dissipation scaled by the theoretical bottom boundary layer shear production, showing increasing variability with increasing stratification for both ADVs.

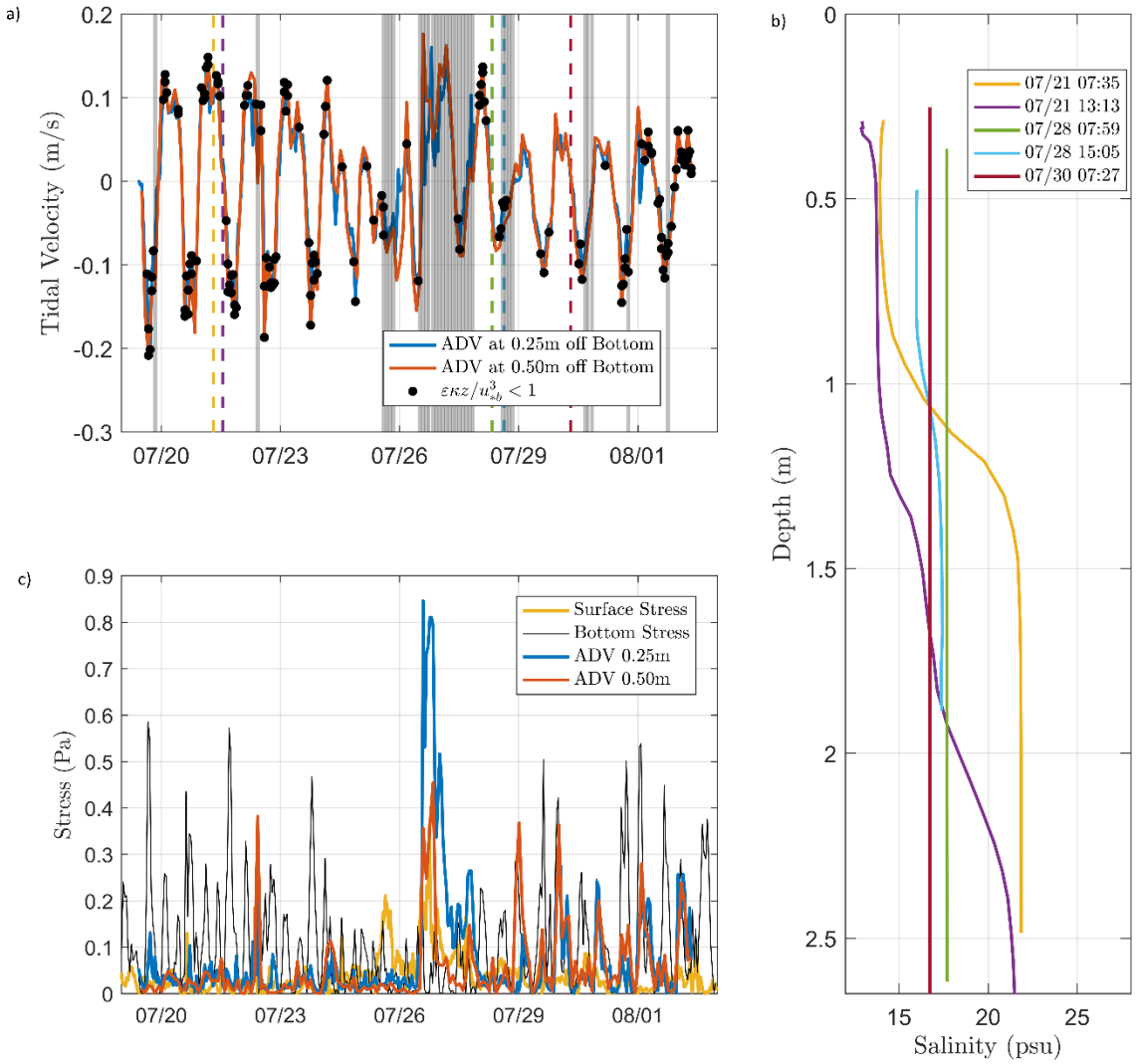

631

632 **Fig. 8** (a) Timeseries velocities (burst averages with positive values indicating flow into the estuary) at both ADVs
633 showing the measured dissipation less than the theoretical prediction for an unstratified boundary layer (black dots)
634 where vertical gray lines denote periods of waves not analyzed in Fig. 7, (b) five salinity profiles taken near the
635 ADV station on July 21, 28, and 30 with the vertical dashed lines in (a) with corresponding colors, and (c)
636 theoretical surface and bottom stress estimates plotted with Reynolds stress values from the ADVs.
637

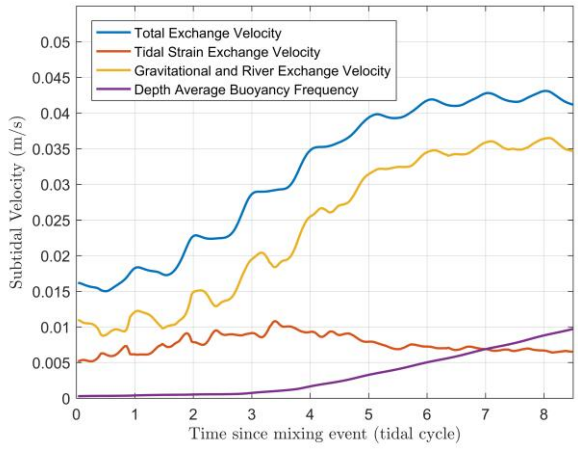

638

639 **Fig. 9** The modeled total exchange velocity and its two components of the tidal straining and the combined
640 gravitational and river discharge components, with the depth average stratification.
641

642

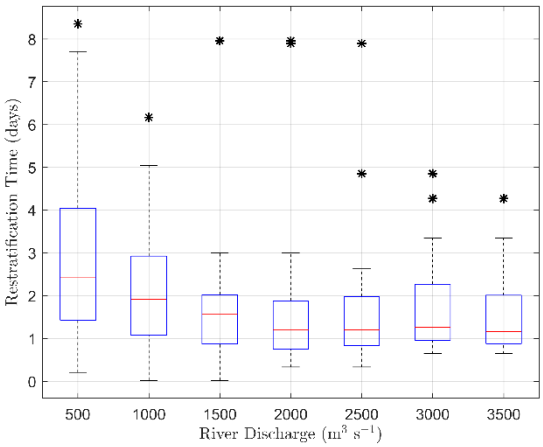

643

644 **Fig. 10** Box plot of bin averaged restratification times estimated using the long-term data from station MB vs. river
645 discharge.
646